

Hydrodynamic evolution and jet energy loss in Cu+Cu collisions

Björn Schenke,^{1,2} Sangyong Jeon,² and Charles Gale²

¹*Physics Department, Bldg. 510A, Brookhaven National Laboratory, Upton, NY 11973, USA*

²*Department of Physics, McGill University, 3600 University Street, Montreal, Quebec, H3A 2T8, Canada*

We present results from a hybrid description of Cu+Cu collisions using 3+1 dimensional hydrodynamics (MUSIC) for the bulk evolution and a Monte-Carlo simulation (MARTINI) for the evolution of high momentum partons in the hydrodynamical background. We explore the limits of this description by going to small system sizes and determine the dependence on different fractions of wounded nucleon and binary collisions scaling of the initial energy density. We find that Cu+Cu collisions are well described by the hybrid description at least up to 20% central collisions.

I. INTRODUCTION

In order to learn about the range of applicability of both hydrodynamics and energy loss mechanisms in heavy-ion collisions, we study Cu+Cu collisions at $\sqrt{s} = 200$ GeV and different centralities. Cu+Cu collisions are ideally suited for this because they are systems with a number of participants that corresponds to that in peripheral Au+Au collisions [1], and can be studied experimentally with reduced uncertainties [2]. One should thus be able to study the transition from “soft” (hydro-like) features to “hard” features (jet-like).

Hydrodynamics assumes that the system is equilibrated within a short time of the order of $\tau_0 = 0.5$ fm/c. This assumption could be fulfilled for central Cu+Cu collisions but is unlikely to hold for peripheral ones. Hence, it is important to study a wide range of centrality classes to see when and for which p_T range the assumption breaks down.

In this work we are able to describe the entire experimentally covered p_T range. The soft or low- p_T sector of the matter produced is described using 3+1D relativistic hydrodynamics (MUSIC [3]) and the hard sector ($p_T \gtrsim 2$ GeV) with the Monte-Carlo simulation MARTINI [4], which uses the hydrodynamic calculation as input and evolves the hard partons in the soft hydrodynamic background with the McGill-AMY (Arnold, Moore and Yaffe) energy loss approach which treats radiative [5, 6] and elastic processes [7].

We can therefore achieve a complete description of Cu+Cu collisions under the assumption that both hydrodynamics and the energy loss formalism are valid. Knowing that we reach the limits of applicability of both models particularly for large centralities, this study allows to pin down observables that are sensitive to a failure of our approach and draw conclusions about the nature of the produced system in Cu+Cu collisions.

II. SOFT PART - HYDRODYNAMICS

To describe the soft part of the matter produced in a heavy-ion collision we employ hydrodynamics. More precisely, we use the ideal 3+1D relativistic implementation of the Kurganov-Tadmor scheme [8] – MUSIC – introduced in [3].

The hydrodynamic equations have the following general form:

$$\partial_t \rho_a = -\nabla \cdot \mathbf{J}_a , \quad (1)$$

where a runs from 0 to 4, labelling the energy, 3 components of the momentum and the net baryon density.

The task is to solve these equations together with the equation of state. The Kurganov-Tadmor (KT) method, combined with a suitable flux limiter, is a non-oscillatory and simple central difference scheme with a small artificial viscosity that can also handle shocks very well. It is Riemann-solver free and hence does not require calculating the local characteristics.

When describing heavy-ion collisions it is useful to employ $\tau - \eta_s$ coordinates defined by

$$\begin{aligned} t &= \tau \cosh \eta_s , \\ z &= \tau \sinh \eta_s . \end{aligned} \quad (2)$$

Then the conservation equation $\partial_\mu J^\mu = 0$ becomes

$$\partial_\tau (\tau J^\tau) + \partial_{\eta_s} J^{\eta_s} + \partial_v (\tau J^v) = 0 , \quad (3)$$

where

$$J^\tau = (\cosh \eta_s J^0 - \sinh \eta_s J^3) , \quad (4)$$

$$J^{\eta_s} = (\cosh \eta_s J^3 - \sinh \eta_s J^0) , \quad (5)$$

which is nothing but a Lorentz boost with the space-time rapidity $\eta_s = \tanh^{-1}(z/t)$. The indices v and w refer to the transverse x, y coordinates which are not affected by the boost. Applying the same transformation to both indices of $T^{\mu\nu}$, one obtains

$$\partial_\tau (\tau T^{\tau\tau}) + \partial_{\eta_s} (T^{\eta_s\tau}) + \partial_v (\tau T^{v\tau}) + T^{\tau\eta_s} = 0 , \quad (6)$$

and

$$\partial_\tau (\tau T^{\tau\eta_s}) + \partial_{\eta_s} (T^{\eta_s\eta_s}) + \partial_v (\tau T^{v\eta_s}) + T^{\tau\eta_s} = 0 , \quad (7)$$

and

$$\partial_\tau (\tau T^{\tau v}) + \partial_{\eta_s} (T^{\eta_s v}) + \partial_w (\tau T^{w v}) = 0 , \quad (8)$$

These 5 equations, namely Eq. (3) for the net baryon current, and Eqs. (6, 7, 8) for the energy and momentum are the equations we solve with the KT scheme described in detail in [3, 8].

To close the set of equations (3, 6, 7, 8) we must provide a nuclear equation of state $\mathcal{P}(\varepsilon, \rho)$ which relates the local thermodynamic quantities. The presented calculations all employ an equation of state extracted from recent lattice QCD calculations [9]. There, several parametrizations of the equation of state which interpolate between the lattice data at high temperature and a hadron-resonance gas in the low temperature region were constructed. We adopt the parametrization “s95p-v1” (and call it EOS-L in the following), where the fit to the lattice data was done above $T = 250$ MeV, and the entropy density was constrained at $T = 800$ MeV to be 95% of the Stefan-Boltzmann value. Furthermore, one “data-point” was added to the fit to make the peak in the trace anomaly higher. See Ref. [9] for more details on this parametrization of the nuclear equation of state.

The initialization of the energy density is done using the Glauber model (see Ref. [10] and references therein): Before the collision the density distribution of the two nuclei is described by a Woods-Saxon parametrization

$$\rho_A(r) = \frac{\rho_0}{1 + \exp[(r - R)/d]}, \quad (9)$$

with $R = 4.163$ fm and $d = 0.606$ fm for Cu nuclei. The normalization factor ρ_0 is set such that $\int d^3r \rho_A(r) = A$. With the above parameters we get $\rho_0 = 0.17$ fm⁻³.

The *nuclear thickness function*

$$T_A(x, y) = \int_{-\infty}^{\infty} dz \rho_A(x, y, z), \quad (10)$$

where $r = \sqrt{x^2 + y^2 + z^2}$, can be used to express both the density of wounded nucleons n_{WN} and binary collisions n_{BC} (see e.g. Ref. [3]). Whether the deposited energy density or entropy density scales with n_{WN} or n_{BC} is not clear from first principles. SPS data suggests that the final state particle multiplicity is proportional to the number of wounded nucleons. At RHIC energies a violation of this scaling was found (the particle production per wounded nucleon is a function increasing with centrality. This is attributed to a significant contribution from hard processes, scaling with the number of binary collisions).

As in [3] the shape of the initial energy density distribution in the transverse plane is parametrized as

$$W(x, y, b) = (1 - \alpha) n_{\text{WN}}(x, y, b) + \alpha n_{\text{BC}}(x, y, b), \quad (11)$$

where α determines the fraction of the contribution from binary collisions, and we will study the effect of different choices for α .

For the longitudinal profile we employ the prescription used in Refs. [11–17]. It is composed of a flat region around $\eta_s = 0$, and of half a Gaussian in the forward and backward direction:

$$H(\eta_s) = \exp \left[-\frac{(|\eta_s| - \eta_{\text{flat}}/2)^2}{2\sigma_{\eta}^2} \theta(|\eta_s| - \eta_{\text{flat}}/2) \right]. \quad (12)$$

The full energy density distribution is then given by

$$\varepsilon(x, y, \eta_s, b) = \varepsilon_0 H(\eta_s) W(x, y, b) / W(0, 0, 0). \quad (13)$$

centrality %	$\langle b \rangle$ [fm]
0-5	1.61
0-6	1.76
0-10	2.28
5-10	2.95
6-15	3.47
10-15	3.83
10-20	4.16
15-20	4.55
15-25	4.82
20-30	5.4
25-35	5.92
30-40	6.4

TABLE I. Average impact parameters in selected centrality classes from the optical Glauber model.

The parameters η_{flat} and σ_{η} are tuned to data and will be quoted below.

The impact parameter b is taken to be the average impact parameter $\langle b \rangle$ for a given centrality class and determined using the optical Glauber model (see e.g. [18]). The obtained values are listed in Table I.

The spectrum of produced hadrons of species i with degeneracy g_i is given by the Cooper-Frye formula [19]:

$$E \frac{dN}{d^3p} = \frac{dN}{dy p_T dp_T d\phi_p} = g_i \int_{\Sigma} f(u^\mu p_\mu) p^\mu d^3\Sigma_\mu, \quad (14)$$

with the distribution function

$$f(u^\mu p_\mu) = \frac{1}{(2\pi)^3} \frac{1}{\exp((u^\mu p_\mu - \mu_i)/T_{\text{FO}}) \pm 1}, \quad (15)$$

where T_{FO} is the freeze-out temperature, u^μ is the flow velocity of the fluid, and the energy is given by the invariant expression $E = u^\mu p_\mu$. In practice, we determine the freeze-out hyper-surface geometrically using a triangulation of the three dimensional hyper-surface that is embedded in four-dimensional space-time. The details of this algorithm are described in Ref. [3].

III. HARD PART - MONTE-CARLO JET EVOLUTION

The hard part of the system is described using the Monte-Carlo simulation MARTINI [4]. At the core of MARTINI lies the McGill-AMY formalism for jet evolution in a dynamical thermal medium. This evolution is governed by a set of coupled Fokker-Planck-type rate equations of the form

$$\frac{dP(p)}{dt} = \int_{-\infty}^{\infty} dk \left(P(p+k) \frac{d\Gamma(p+k, k)}{dk} - P(p) \frac{d\Gamma(p, k)}{dk} \right) \quad (16)$$

where $d\Gamma(p, k)/dk$ is the transition rate for processes where partons of energy p lose energy k .

In the finite temperature field theory approach of AMY, radiative transition rates can be calculated by means of integral equations [6] which correctly reproduce both the Bethe-Heitler and the LPM results in their respective limits [20]. Transition rates for the processes $g \rightarrow gg$, $q(\bar{q}) \rightarrow q(\bar{q})g$, and $g \rightarrow q\bar{q}$ are included as well as elastic processes employing the transition rates computed in [7]. Furthermore, gluon-quark and quark-gluon conversion due to Compton and annihilation processes, as well as the QED processes of photon radiation $q \rightarrow q\gamma$ and jet-photon conversions [21, 22] are implemented.

In MARTINI, Eq. (16) is solved using Monte Carlo methods, keeping track of each individual parton, rather than the probability distributions P . This method provides information on the full microscopic event configuration in the high momentum regime, including correlations, which allows for a very detailed analysis and offers a direct interface between theory and experiment.

In a full heavy-ion event, the number of individual nucleon-nucleon collisions that produce partons with a certain minimal transverse momentum p_T^{\min} is determined from the total inelastic cross-section, provided by PYTHIA, which is also used to generate those individual hard collisions. The initial transverse positions of the hard collisions are determined by the initial jet density distribution

$$\mathcal{P}_{AB}(b, \mathbf{r}_\perp) = \frac{T_A(\mathbf{r}_\perp + \mathbf{b}/2)T_B(\mathbf{r}_\perp - \mathbf{b}/2)}{T_{AB}(b)}, \quad (17)$$

which is determined by the nuclear thickness (10) and overlap functions

$$T_{AB}(b) = \int d^2r_\perp T_A(\mathbf{r}_\perp)T_B(\mathbf{r}_\perp + \mathbf{b}). \quad (18)$$

The initial parton distribution functions can be selected with the help of the Les Houches Accord PDF Interface (LHAPDF) [23]. Isospin symmetry is assumed and nuclear effects on the parton distribution functions are included using the EKS98 [24] parametrization.

As discussed above, the soft medium is described by hydrodynamics. Before the hydrodynamic evolution begins ($\tau < \tau_0$), the partons shower as in vacuum. During the medium evolution, individual partons move through the background according to their velocity. Probabilities to undergo an interaction are determined in the local fluid cell rest frame using the transition rates and the local temperature. The boost into the local fluid rest frame is performed using the flow velocities provided by the hydro calculation.

If a process occurs, the radiated or transferred energy is sampled from the transition rate of that process. In case of an elastic process, the transferred transverse momentum is also sampled, while for radiative processes collinear emission is assumed.

Radiated partons are further evolved if their momentum is above a certain threshold $p_{\min} \simeq 2 - 3 \text{ GeV}$. The overall evolution of a parton stops once its energy in a fluid cell's rest frame falls below the limit of $4T$,

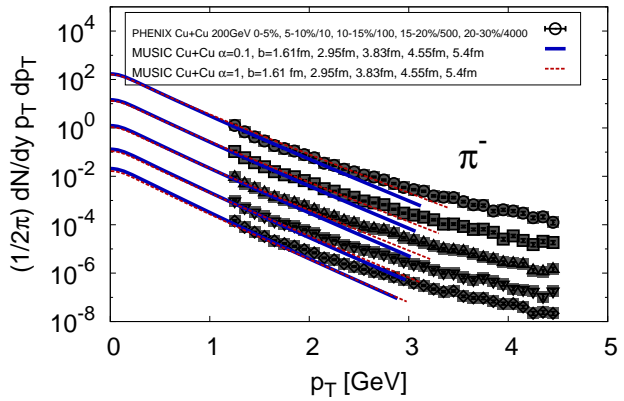


FIG. 1. Transverse momentum spectra of negative pions for different centrality classes compared to preliminary PHENIX data. The collisions go from central (top) to more peripheral (bottom).

where T is the local temperature. For partons that stay above that threshold, the evolution ends once they enter the hadronic phase of the background medium. In the mixed phase or a crossover region, processes occur only for the QGP fraction. When all partons have left the QGP phase, hadronization is performed by PYTHIA, to which the complete information on all final partons is passed. Because PYTHIA uses the Lund string fragmentation model [25, 26], it is essential to keep track of all color strings during the in-medium evolution. For more information on the details of MARTINI please refer to [4].

IV. RESULTS

We begin by presenting results for the soft transverse momentum region obtained entirely by MUSIC. We always compare three different parametrizations, which essentially differ by the contribution of binary collision scaling of the initial energy density distribution (see Eq. (11)). The details of the parameter sets are listed in Table II.

Fig. 1 shows the transverse momentum spectra of negative pions for different centralities compared to preliminary data from PHENIX (see e.g. [27]). For the most central collisions both parametrizations describe the experimental data reasonably well for $p_T \lesssim 2 \text{ GeV}$. The larger the impact parameter, the lower the p_T at which the description using hydrodynamics fails. For 20-30% central collisions the calculation begins to deviate from the experimental data at approximately $p_T \gtrsim 1.5 \text{ GeV}$. Generally, the calculation with larger α leads to harder spectra. For anti-protons we find a very similar behavior, shown in Fig. 2. In this case the result is generally

α	τ_0 [fm]	ε_0 [GeV/fm 3]	ε_{FO} [GeV/fm 3]	T_{FO} [MeV]	η_{flat}	σ_η
0.1	0.55	20	0.14	≈ 140	4	1.2
0.5	0.55	26	0.14	≈ 140	4	1.2
1	0.55	29	0.14	≈ 140	4	1.2

TABLE II. Parameter sets.

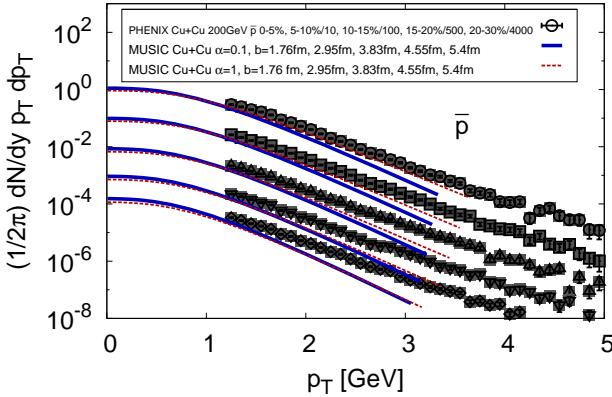


FIG. 2. Transverse momentum spectra of anti-protons for different centrality classes compared to preliminary PHENIX data. The experimental data is underestimated because of the assumption of chemical equilibrium.

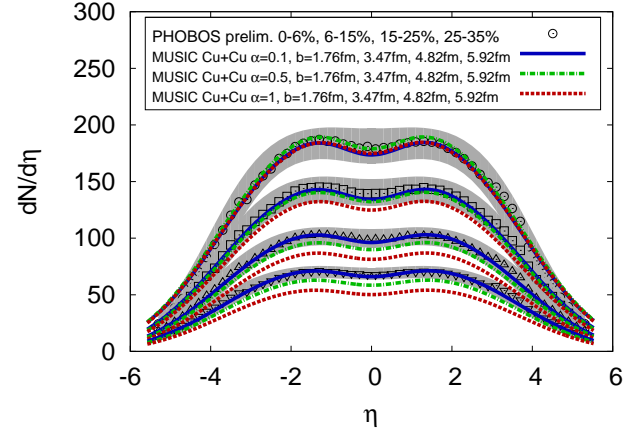


FIG. 3. Centrality dependence of pseudorapidity distributions of charged hadrons compared to preliminary PHOBOS data [30] (open symbols). Calculations using $\alpha = 0.1$ describe all centrality classes very well, while larger α lead to deviations for larger centralities.

below the data because of the assumed chemical equilibrium (see Ref. [3]), the overall shape of the spectra is however well reproduced for low p_T .

Although we find harder spectra in the case of $\alpha = 1$ it is unclear which parametrization is favored solely by studying the p_T spectra of pions and anti-protons. The centrality dependence of charged particle pseudo-rapidity distributions in Fig. 3 reveals a much more obvious difference. While in the case $\alpha = 0.1$ the experimental data is very well described for all shown centrality classes, the calculations using $\alpha = 0.5$ and $\alpha = 1$ only describe the most central data to which the parameters were adjusted, but differ increasingly with increasing impact parameter.

It is remarkable how well the p_T integrated pseudorapidity distributions are described even for very large pseudorapidities and impact parameters. This indicates that for low p_T , i.e., $p_T \lesssim 1$ GeV, hydrodynamics works well, hinting at that the low momentum modes equilibrate fast enough even in small systems, while higher momentum modes do not.

Next, we present the elliptic flow parameter v_2 and compare to STAR data [28]. Because we do not include fluctuations, we do not expect the centrality dependence of elliptic flow to be reproduced. See Ref. [29] for a demonstration of the importance of fluctuations on elliptic flow observables. In Fig. 4 we show results for 10-20% central events, a centrality class in which $v_2(p_T)$ was found to be well described by smooth initial condi-

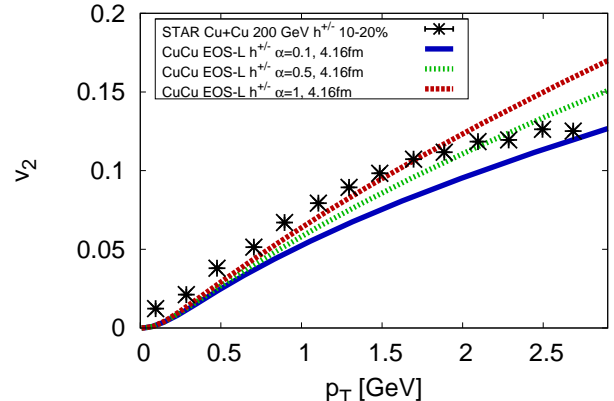


FIG. 4. Elliptic flow coefficient v_2 as a function of transverse momentum for 10-20% central events compared to STAR data [28].

tions, at least for Au+Au collisions [29]. The dependence on the α parameter is as expected. Larger α meaning higher initial eccentricity, leads to stronger elliptic flow. To draw further conclusions from this comparison a detailed event-by-event study is needed.

Extracting the evolution information from the hydrodynamic simulation, i.e., the temperature and flow veloc-

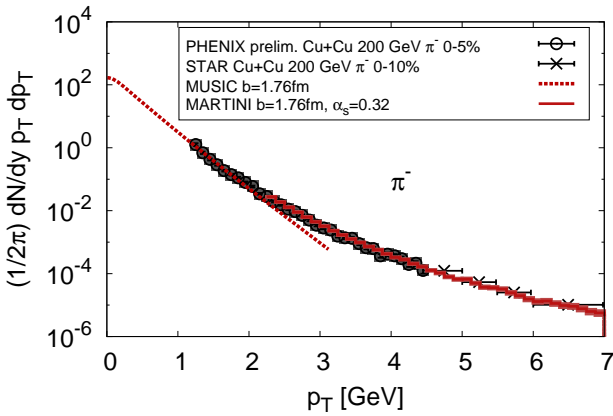


FIG. 5. Transverse momentum spectrum of negative pions from the hydrodynamic calculation MUSIC (dashed line) and MARTINI using MUSIC input (solid line) compared to data from PHENIX (preliminary) and STAR [31].

ties as functions of time and spatial coordinates, we can use this information as an input for the simulation of the evolution of the hard degrees of freedom, MARTINI.

This way we can compute the hard part of the spectrum and combine results for the soft and hard part as done in Fig. 5 for negative pions. The additional free parameter that regulates the amount of energy loss in MARTINI is the strong coupling constant, which we fix at $\alpha_s = 0.32$. The value of transverse momentum up to where hydrodynamics alone provides a good description and beyond which the contribution from jets becomes important decreases with decreasing system size. For central Au+Au collisions the value lies between 3 and 4 GeV [3], while Fig. 5 shows that for Cu+Cu it lies around 2 GeV for central collisions, and from Fig. 1 one can read off that it decreases more when going to larger centralities.

Next, we study the nuclear modification factor for neutral pions, defined by

$$R_{AA} = \frac{1}{N_{\text{coll}}(b)} \frac{dN_{AA}(b)/d^2 p_T dy}{dN_{pp}/d^2 p_T dy}, \quad (19)$$

where $N_{\text{coll}}(b)$ is the number of binary collisions at given impact parameter b . The reference spectrum $dN_{pp}/d^2 p_T dy$ for p+p collisions was computed in [4].

Figures 6 to 9 show the nuclear modification factor R_{AA} for different centrality classes. The value of α_s was chosen to match the experimental data in the most central collisions best, but when going to larger centrality classes the impact parameter is the only quantity that is changed. We see that all hydrodynamic backgrounds ($\alpha \in \{0.1, 0.5, 1\}$) lead to good agreement with the experimental data in the two most central bins (Figs. 6 and 7). All calculations, but most significantly the one using $\alpha = 0.1$, deviate from the 20-30% and 30-40% central experimental data. This indicates that the combination

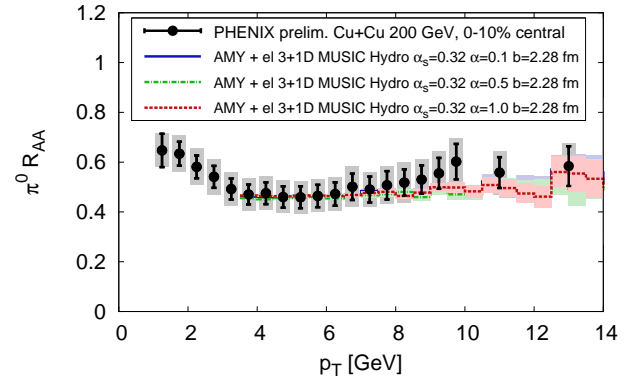


FIG. 6. Nuclear modification factor for neutral pions in 0-10% central Cu+Cu collisions compared to preliminary data from PHENIX.

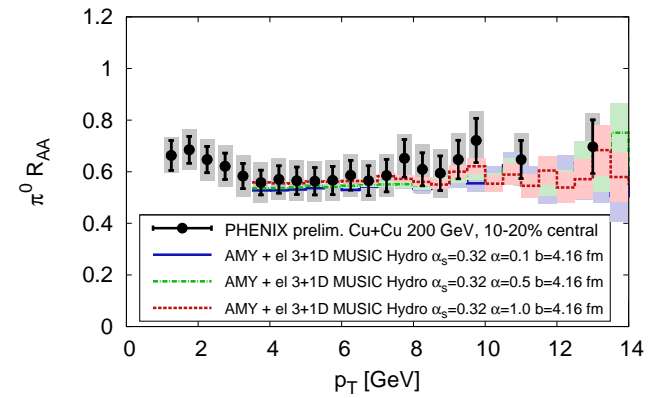


FIG. 7. Nuclear modification factor for neutral pions in 10-20% central Cu+Cu collisions compared to preliminary data from PHENIX.

of ideal hydrodynamics with our energy loss mechanism begins to fail to describe Cu+Cu systems at centralities $\gtrsim 20\%$. Remember that hydrodynamics using $\alpha = 0.1$ described the bulk data well, while deviations from experimental data at more peripheral collisions are large for $\alpha = 0.5$ and $\alpha = 1$ (Fig. 3).

On the other hand $\alpha = 1$ works best for R_{AA} . This indicates that the energy loss mechanism itself leads to a too weak centrality dependence when using the “correct” hydrodynamic background ($\alpha = 0.1$). Using a hydrodynamic background with a larger centrality dependence of the density ($\alpha = 1$) then works against this problem. Note, however, that for all α the results for R_{AA} lie within the experimental error bars. The effect of non-zero viscosity and event-by-event fluctuations [29] remains to be studied.

Finally we study high momentum photon production in Cu+Cu collisions. Photons in the high p_T region produced in nuclear collisions are dominantly direct photons,

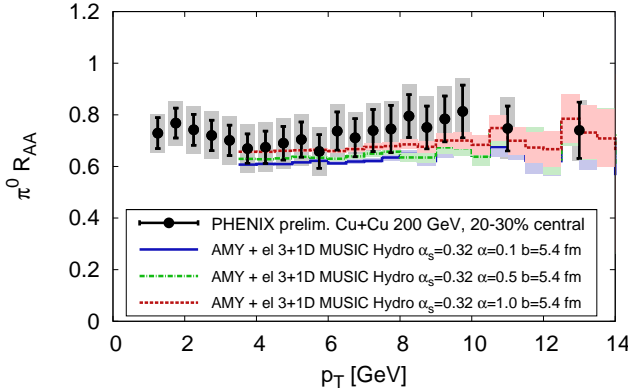


FIG. 8. Nuclear modification factor for neutral pions in 20-30% central Cu+Cu collisions compared to preliminary data from PHENIX.

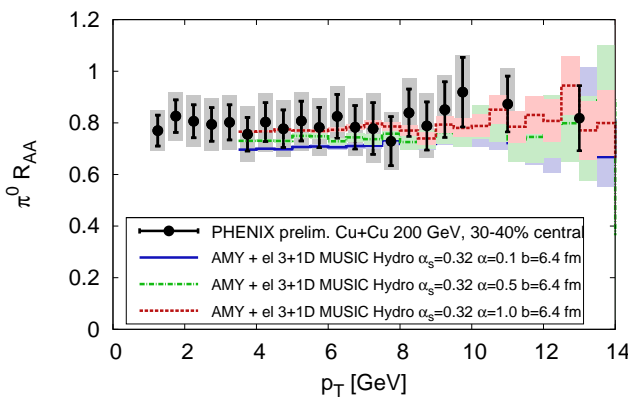


FIG. 9. Nuclear modification factor for neutral pions in 30-40% central Cu+Cu collisions compared to preliminary data from PHENIX.

fragmentation photons, and jet-plasma photons. Direct photons are included in PYTHIA. Apart from leading order direct photons, PYTHIA produces additional photons emitted during the vacuum showers, which in part overlap with photons from next-to-leading order calculations. Fragmentation photons are also part of those produced in the shower. For heavy-ion reactions MARTINI adds the very relevant jet-medium photons from photon radiation $q \rightarrow q\gamma$ (bremsstrahlung photons) and jet-photon conversion via Compton and annihilation processes. The full vacuum shower is included in the calculation - most of the shower photons will be emitted before the medium has formed and the parton has realized that it has formed. For more details on the implementation see [4].

In Fig. 10 we present the nuclear modification factor for photons compared to preliminary data from PHENIX (also see [27]) in central collisions. Again, the reference spectrum from p+p collisions was computed in [4]. The

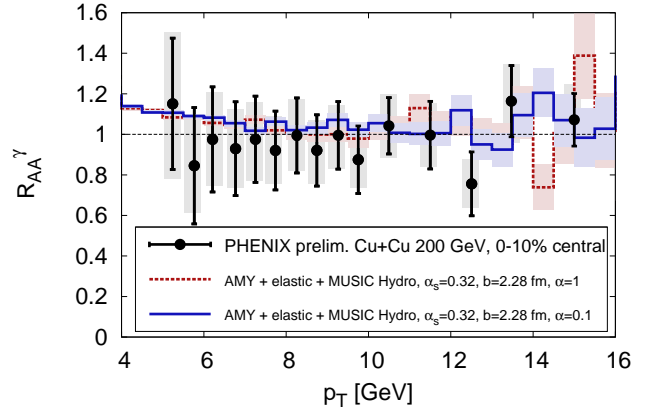


FIG. 10. Nuclear modification factor for photons in 0-10% central Cu+Cu collisions compared to preliminary data from PHENIX.

data is consistent with $R_{AA}^{\gamma} = 1$ and so is the calculation for a wide range of p_T . The rise above one for $p_T \lesssim 6$ GeV stems from the contribution of in-medium photon production. Unfortunately the current experimental data does not allow to distinguish whether this contribution is present or not.

V. CONCLUSIONS AND OUTLOOK

We studied the applicability of both a 3+1D hydrodynamic model and the McGill-AMY jet energy loss and evolution scheme to Cu+Cu collisions of different centralities. Because the created system is smaller than in Au+Au collisions the limits of the models are already reached at a smaller impact parameter. The precise determination of these limits and the determination of observables that are sensitive to the failing of the models was the main objective of this work.

The hydrodynamic evolution was computed using the relativistic 3+1D implementation of the Kurganov-Tadmor scheme, dubbed MUSIC, while the evolution of the hard degrees of freedom was simulated using the Monte-Carlo simulation MARTINI. With these, we were able to compare calculations to experimental observables over the full range of measured transverse momentum.

As expected, the quality of the description of transverse momentum spectra of identified hadrons using only hydrodynamics depends on the system size. While in Au+Au collisions the spectra in central collisions are typically well described up to $p_T \approx 3$ GeV, in Cu+Cu we find deviations at approximately 2 GeV for central collisions, and lower p_T for larger centralities.

The hydrodynamic calculation of the centrality dependence of pseudorapidity distributions agrees very well with the experimental data when we use 90% wounded nucleon scaling and 10% binary collisions scaling of the

initial energy density distribution. The parameter set using 100% binary collision scaling does not reproduce the centrality classes above 10%. We therefore conclude that mostly wounded nucleon scaling provides a better description of experimental data. In this case, the result shows that the low transverse momentum modes that dominate the distribution are thermalized, even in 30-40% central collisions, which is in agreement with the result for the transverse momentum spectra.

Including the contribution from jets by employing MARTINI, which uses the hydrodynamic evolution as input, we were able to describe the complete pion spectra in central collisions. The study of R_{AA} for pions allows to pin down the point where the combined ideal hydrodynamics+McGill-AMY evolution breaks down.

The trend seen in the description of the centrality dependence of R_{AA} agrees least with experimental data when using $\alpha = 0.1$, which is preferred by the low momentum spectra. While calculations for 0-10% and 10-

20% central bins agree well with experimental data, deviations begin for centralities larger than 20%. This might indicate that the used energy loss mechanism does not have the correct density and/or system size dependence for the small systems studied here. The current error bars do not permit a more precise quantitative statement.

ACKNOWLEDGMENTS

B.P.S. thanks Roy Lacey for help with locating the experimental data. This work was supported in part by the Natural Sciences and Engineering Research Council of Canada. B.P.S. gratefully acknowledges a Richard H. Tomlinson Postdoctoral Fellowship by McGill University. B.P.S. was supported in part by the US Department of Energy under DOE Contract No. DE-AC02-98CH10886, and by a Lab Directed Research and Development Grant from Brookhaven Science Associates.

[1] S. S. Adler *et al.* (PHENIX), Phys. Rev. Lett., **91**, 072301 (2003), arXiv:nucl-ex/0304022.

[2] A. Adare *et al.* (PHENIX), Phys. Rev. Lett., **101**, 162301 (2008), arXiv:0801.4555 [nucl-ex].

[3] B. Schenke, S. Jeon, and C. Gale, (2010), arXiv:1004.1408 [hep-ph].

[4] B. Schenke, C. Gale, and S. Jeon, Phys. Rev., **C80**, 054913 (2009), arXiv:0909.2037 [hep-ph].

[5] P. Arnold, G. D. Moore, and L. G. Yaffe, JHEP, **12**, 009 (2001).

[6] P. Arnold, G. D. Moore, and L. G. Yaffe, JHEP, **06**, 030 (2002).

[7] B. Schenke, C. Gale, and G.-Y. Qin, Phys. Rev., **C79**, 054908 (2009).

[8] A. Kurganov and E. Tadmor, Journal of Computational Physics, **160**, 214 (2000).

[9] P. Huovinen and P. Petreczky, (2009), arXiv:0912.2541 [hep-ph].

[10] M. L. Miller, K. Reygers, S. J. Sanders, and P. Steinberg, Ann. Rev. Nucl. Part. Sci., **57**, 205 (2007), arXiv:nucl-ex/0701025.

[11] T. Ishii and S. Muroya, Phys. Rev., **D46**, 5156 (1992).

[12] K. Morita, S. Muroya, H. Nakamura, and C. Nonaka, Phys. Rev., **C61**, 034904 (2000), arXiv:nucl-th/9906037.

[13] T. Hirano, K. Morita, S. Muroya, and C. Nonaka, Phys. Rev., **C65**, 061902 (2002), arXiv:nucl-th/0110009.

[14] T. Hirano, Phys. Rev., **C65**, 011901 (2002), arXiv:nucl-th/0108004.

[15] T. Hirano and K. Tsuda, Phys. Rev., **C66**, 054905 (2002), arXiv:nucl-th/0205043.

[16] K. Morita, S. Muroya, C. Nonaka, and T. Hirano, Phys. Rev., **C66**, 054904 (2002), arXiv:nucl-th/0205040.

[17] C. Nonaka and S. A. Bass, Phys. Rev., **C75**, 014902 (2007).

[18] H. Niemi, K. J. Eskola, and P. V. Ruuskanen, Phys. Rev., **C79**, 024903 (2009), arXiv:0806.1116 [hep-ph].

[19] F. Cooper and G. Frye, Phys. Rev., **D10**, 186 (1974).

[20] S. Jeon and G. D. Moore, Phys. Rev., **C71**, 034901 (2005).

[21] R. J. Fries, B. Muller, and D. K. Srivastava, Phys. Rev. Lett., **90**, 132301 (2003).

[22] S. Turbide, C. Gale, E. Frodermann, and U. Heinz, Phys. Rev., **C77**, 024909 (2008).

[23] M. R. Whalley, D. Bourilkov, and R. C. Group, (2005), arXiv:hep-ph/0508110.

[24] K. J. Eskola, V. J. Kolhinen, and C. A. Salgado, Eur. Phys. J., **C9**, 61 (1999).

[25] B. Andersson, G. Gustafson, G. Ingelman, and T. Sjstrand, Phys. Rept., **97**, 31 (1983).

[26] T. Sjstrand, Nucl. Phys., **B248**, 469 (1984).

[27] T. Chujo (PHENIX), J. Phys., **G34**, S893 (2007), arXiv:nucl-ex/0703014.

[28] B. I. Abelev *et al.* (The STAR), Phys. Rev., **C81**, 044902 (2010), arXiv:1001.5052 [nucl-ex].

[29] B. Schenke, S. Jeon, and C. Gale, (2010), arXiv:1009.3244 [hep-ph].

[30] G. I. Veres *et al.* (PHOBOS Collaboration), (2008), arXiv:0806.2803 [nucl-ex].

[31] B. I. Abelev *et al.* (STAR), (2009), arXiv:0911.3130 [nucl-ex].